Second-order nonlinear Schrödinger equation breather solutions in the degenerate and rogue wave limits

David J. Kedziora,* Adrian Ankiewicz, and Nail Akhmediev
Optical Sciences Group, Research School of Physics and Engineering, The Australian National University, Canberra ACT 0200, Australia
(Received 17 January 2012; published 4 June 2012)

We present an explicit analytic form for the two-breather solution of the nonlinear Schrödinger equation with imaginary eigenvalues. It describes various nonlinear combinations of Akhmediev breathers and Kuznetsov-Ma solitons. The degenerate case, when the two eigenvalues coincide, is quite involved. The standard inverse scattering technique does not generally provide an answer to this scenario. We show here that the solution can still be found as a special limit of the general second-order expression and appears as a mixture of polynomials with trigonometric and hyperbolic functions. A further restriction of this particular case, where the two eigenvalues are equal to i, produces the second-order rogue wave with two free parameters considered as differential shifts. The illustrations reveal a precarious dependence of wave profile on the degenerate eigenvalues and differential shifts. Thus we establish a hierarchy of second-order solutions, revealing the interrelated nature of the general case, the rogue wave, and the degenerate breathers.

DOI: 10.1103/PhysRevE.85.066601 PACS number(s): 05.45.Yv, 47.20.Ky, 42.65.−k

I. INTRODUCTION

Breather solutions of certain nonlinear equations are presently well accepted as potential prototypes for the notorious rogue waves in the ocean [1–9] and other fields of physics [10–12]. Breathers develop due to the instability of small amplitude perturbations that may grow in size to disastrous proportions. As the perturbations are usually chaotic and may contain many frequencies in their spectra, an important issue is our ability to construct higher-order solutions that grow as a nonlinear superposition of several lowest-order breathers [13,14]. Numerically, such solutions can be constructed with ease, and this has been done in a number of previous publications [14,15]. Analytic expressions for these solutions are another matter. They are usually cumbersome and admit many forms. Finding the simplest one is always a challenge.

In this work, we provide the two-breather solution of the nonlinear Schrödinger equation (NLSE) in explicit form. The solution has two eigenvalues as variable parameters of the breathers, thus allowing for a variety of particular cases. Of special interest is the case when the two eigenvalues coincide. The answer provided by the standard inverse scattering technique then becomes undefined. Nevertheless, the solution still does exist but requires special methods to reveal it. This procedure is analogous to the method employed with two-soliton solutions [16,17] where the degenerate case also requires a special approach. These techniques are highly nontrivial, but the final results are usually simpler than we may expect. They appear as a mixture of polynomials with trigonometric and hyperbolic functions.

The general solution with one, two, or more eigenvalues can be obtained using a variety of techniques including Darboux transformations [18]. This is the methodology that we use in this work. Having an explicit analytic solution has the advantage that we can also consider all particular cases analytically, including the rational solutions that have been studied in a number of recent works [19–24]. These include higher-order rogue waves [19,20] and their varied forms [21–27]. In our present approach, rational solutions are just one of the limiting cases of the two-breather solution. A superposition of breathers that create a rogue wave can also be considered [14]. Thus our approach here is quite general. It provides a comprehensive understanding of second-order NLSE breather solutions and their hierarchical nature.

The NLSE can be written in dimensionless form as

$$i\frac{\partial\psi}{\partial x}+\frac{1}{2}\frac{\partial^2\psi}{\partial t^2}+|\psi|^2\psi=0. \tag{1}$$

The wave function $|\psi(x,t)|$ in Eq. (1) commonly describes the wave envelope. In fiber optic applications [12], the variable x is the distance along the fiber while t is the retarded time in the frame moving with the pulse group velocity. On the other hand, in water wave applications [9], x is the dimensionless time while t is the distance in the frame moving with the group velocity. Such a difference is more related to traditions in each field rather than to any particular physical meaning. Simple linear transformation between the variables involving the group velocity allows us to change the equation and variables from one form to another.

There is a class of first-order solutions to Eq. (1), pertaining to modulation instability [28], that can be described by a complex eigenvalue l [29]. The real part of the eigenvalue represents the angle that the one-dimensionally localized solutions form with the x axis, and the imaginary part characterizes the frequency of periodic modulation. A variety of different forms for this solution has been given in several publications by different authors [14,30–33]. The case of complex eigenvalues is rather involved and numerical results [15] may be easier to comprehend than analytic solutions. In this work, we restrict our analysis to purely imaginary eigenvalues, thus allowing us to present and analyze the second-order solutions in a relatively simple way.

The general form of the first-order breather solution [34] is

$$\psi=\left[\frac{\kappa^2\cosh\delta(x-x_1)+2i\kappa\nu\sinh\delta(x-x_1)}{2[\cosh\delta(x-x_1)-\nu\cos\kappa(t-t_1)]}-1\right]e^{ix}, \tag{2}$$

*djk105@rsphysse.anu.edu.au

where $\nu = \mathrm{Im}(l)$, $\kappa = 2\sqrt{1+l^2}$, and both x_1 and t_1 serve as coordinate shifts from the origin. The dependent variable $\delta = \kappa\nu$ in this expression is the growth rate of modulation instability; this is the process occurring as the plane wave evolves from a small periodic perturbation at $x = -\infty$.

When $0 < \nu < 1$ and κ is real, the solution is a t-periodic wave function that is localized in x, currently known as an Akhmediev breather (AB) [2,6,7]. This solution has been illustrated earlier in Fig. 1(a) of Ref. [27]. On the other hand, when $\nu > 1$ and κ is imaginary, the trigonometric (dependent on t) and hyperbolic (dependent on x) functions in Eq. (2) convert to their analogues via the relations

$$\sinh(z) = -i\sin(iz) \quad \text{and} \quad \cosh(z) = \cos(iz). \tag{3}$$

Taking into account these transformations, we obtain a soliton solution in the following form:

$$\psi = \left[\frac{-p^2\cos\Omega(x-x_1) - 2ip\nu\sin\Omega(x-x_1)}{2[\cos\Omega(x-x_1) - \nu\cosh p(t-t_1)]} - 1\right] e^{ix}, \tag{4}$$

where $\kappa = ip$, $p = 2\sqrt{\nu^2-1}$, and $\delta = i\Omega$, $\Omega = p\nu$. This is a soliton on a background, localized in t and periodic in x. It is known as a Kuznetsov [35] or Ma [36] (KM) soliton and has previously been presented in Fig. 1(b) of Ref. [27].

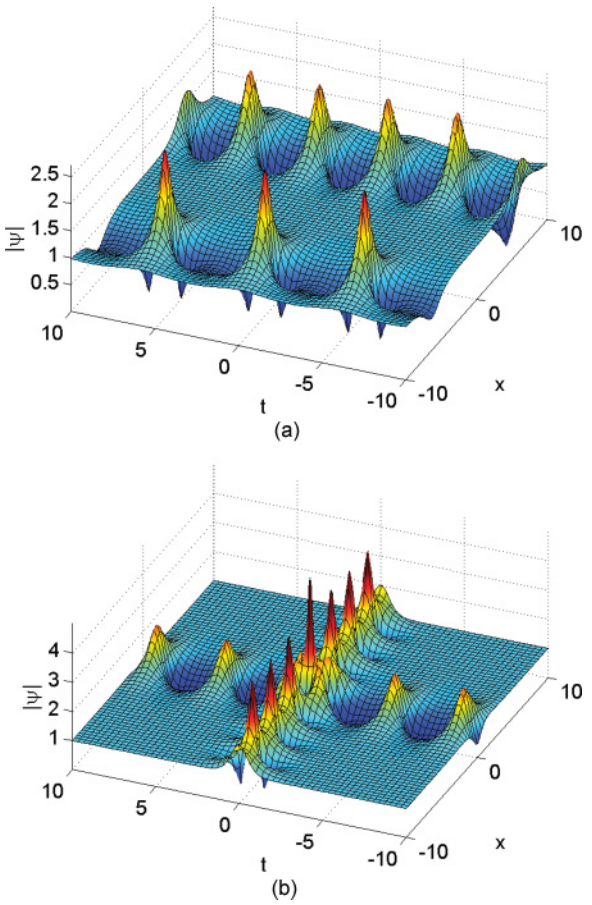

FIG. 1. (Color online) Various forms of second-order NLSE solution with different eigenvalues l_j. (a) Nonlinear superposition of two ABs with $l_1 = 0.65i$ and $l_2 = 0.85i$. Finite shifts are $x_1 = 5$ and $x_2 = -5$. (b) An AB with $l_1 = 0.65i$ crossing a KM soliton with $l_2 = 1.35i$.

Equations (2) and (4) represent an AB and a KM soliton, respectively, with the frequency parameters κ and Ω being real values in each case. One is the analytic continuation of the other when the parameter ν passes through the point 1. Each solution can be written in the general form below with real G_n, H_n, and D_n [see Eq. (5)]. In what follows, we take this fact into account and assume, in several equations below, that coefficients may take real or imaginary values, thus avoiding the need to explicitly present several real-coefficient versions of the same solution. When loaded into modern software such as MATLAB, the assumption of complex coefficients allows these equations to be computed correctly without the need for further specifications.

In the nontrivial limit, when $\nu \to 1$ or $\kappa \to 0$, the above expressions become undefined. However, this problem can be resolved using l'Hôpital's rule. Then, the period of either solution goes to infinity and the resulting wave function is the Peregrine soliton localized in both x and t. It was shown earlier in Fig. 1(c) of Ref. [27]. This solution is also known as a first-order rogue wave. Using the general form

$$\psi_n(x,t) = \left[(-1)^n + \frac{G_n + i\,H_n}{D_n}\right] e^{ix} \tag{5}$$

to represent a NLSE solution of order n, this rational solution has the values for G_1, H_1, and D_1 given by

$$\begin{aligned} &G_1 = 4, \quad H_1 = 8(x-x_1), \\ &D_1 = 1 + 4(x-x_1)^2 + 4(t-t_1)^2. \end{aligned} \tag{6}$$

NLSE breather solutions take the above simple forms only when the real part of the eigenvalues is zero. The general case of complex eigenvalues is significantly more complicated, but the method and low-order analytic results have previously been presented (see the appendix of Ref. [14]).

II. TWO-BREATHER SOLUTION IN GENERAL FORM

Various methods exist for generating higher-order NLSE solutions that exist on a background plane wave. We employ the recursive Darboux method [13,18], which nonlinearly superimposes distinct components of AB or KM soliton form. Each first-order component j in the higher-order solution is described by the (imaginary) eigenvalue l_j, the modulation frequency $\kappa_j = 2\sqrt{1+l_j^2}$, and a shifted point of origin (x_j, t_j). A detailed step-by-step description of this technique has been presented previously (see the appendix of Ref. [27]). For convenience, we define $x_{sj} = x - x_j$ and $t_{sj} = t - t_j$ as shifted variables.

With these parameters, we find that the general solution can be written in the same form as Eq. (5), but with the values for G_2, H_2, and D_2 given by

$$\begin{aligned} G_2 = -\left(\kappa_1^2 - \kappa_2^2\right)\Bigg(&\frac{\kappa_1^2\delta_2}{\kappa_2}\cosh(\delta_1 x_{s1})\cos(\kappa_2 t_{s2}) \\ &- \frac{\kappa_2^2\delta_1}{\kappa_1}\cosh(\delta_2 x_{s2})\cos(\kappa_1 t_{s1}) \\ &- \left(\kappa_1^2 - \kappa_2^2\right)\cosh(\delta_1 x_{s1})\cosh(\delta_2 x_{s2})\Bigg), \end{aligned}$$

$$
\begin{aligned}
H_2 = {} & -2\left(\kappa_1^2-\kappa_2^2\right)\Bigg(\frac{\delta_1\delta_2}{\kappa_2}\sinh(\delta_1 x_{s1})\cos(\kappa_2 t_{s2}) \\
& -\frac{\delta_1\delta_2}{\kappa_1}\sinh(\delta_2 x_{s2})\cos(\kappa_1 t_{s1}) \\
& -\delta_1\sinh(\delta_1 x_{s1})\cosh(\delta_2 x_{s2}) \\
& +\delta_2\sinh(\delta_2 x_{s2})\cosh(\delta_1 x_{s1})\Bigg), \\
D_2 = {} & 2\left(\kappa_1^2+\kappa_2^2\right)\frac{\delta_1\delta_2}{\kappa_1\kappa_2}\cos(\kappa_1 t_{s1})\cos(\kappa_2 t_{s2}) \\
& +4\delta_1\delta_2\Big(\sin(\kappa_1 t_{s1})\sin(\kappa_2 t_{s2}) \\
& +\sinh(\delta_1 x_{s1})\sinh(\delta_2 x_{s2})\Big) \\
& -\left(2\kappa_1^2-\kappa_1^2\kappa_2^2+2\kappa_2^2\right)\cosh(\delta_1 x_{s1})\cosh(\delta_2 x_{s2}) \\
& -2\left(\kappa_1^2-\kappa_2^2\right)\Bigg(\frac{\delta_1}{\kappa_1}\cos(\kappa_1 t_{s1})\cosh(\delta_2 x_{s2}) \\
& -\frac{\delta_2}{\kappa_2}\cos(\kappa_2 t_{s2})\cosh(\delta_1 x_{s1})\Bigg),
\end{aligned}
\tag{7}
$$

where the instability growth rate for each component is $\delta_j = \kappa_j\sqrt{4-\kappa_j^2}/2$. A special case of this solution, where the two frequencies of modulation are harmonics of each other, has been given previously in Ref. [34]. We stress here that the two frequencies are independent parameters of the solution. Moreover, this present solution includes both ABs and KM solitons in any combination. To have an explicit real-parameter form for the cases when one or two values of $\nu_j = \mathrm{Im}(l_j)$ are greater than 1 (or the corresponding κ_j values are imaginary), we can again apply the relations in Eq. (3) to Eq. (7).

Thus, within the set of solutions with purely imaginary eigenvalues, Eqs. (5) and (7) are capable of describing a variety of possible second-order cases. For example, the case of one AB developing with a time delay after another is shown in Fig. 1(a), where both have different modulation frequencies. Alternatively, the intersection of an AB with a KM soliton is shown in Fig. 1(b). These two examples demonstrate that our second-order solution is a versatile tool for modeling the nonlinear superposition of two arbitrary ABs, KM solitons, or their combinations. This idea has previously been explored with the concept of rogue waves being formed from colliding ABs [14]. Despite the fact that our present solution is a particular case of complex eigenvalues, it is presented here in a simple explicit analytic form. Two more examples are shown in Fig. 2. These are combinations of two ABs located at the same position in x and t, but with different frequencies.

Generally, second-order solutions of the NLSE do not admit two equal eigenvalues, otherwise the analytic expressions become undefined. Our present solution given by Eqs. (5) and (7) is not an exception. Moreover, none of the eigenvalues in the above expressions can be equal to i. It can easily be seen that in these cases, G_2, H_2, and D_2 are zero, and the analytic expression has to be further modified in order to be presented in explicit form.

These problems are complicated but can be surmounted by applying analytic limits. As demonstrated for the first-order solution in Sec. I, taking the limit $l_j \to i$ is the key to accessing important rational rogue wave solutions. In order to avoid the case of equal eigenvalues, we can, as in previous work [27], choose to set $\kappa_j = j\kappa$ and then apply the $\kappa \to 0$ limit. This trick effectively extends the period of the wave function shown in Fig. 2(a) to infinity, leaving behind only the central second-order rogue wave peak. This technique ensures that the component eigenvalues are distinct all the way to the $l_j = i$ limit.

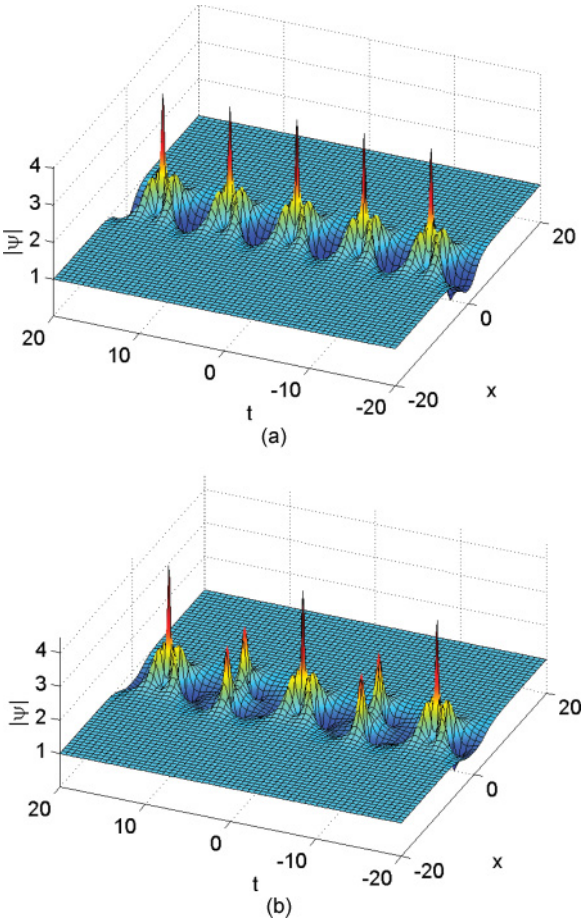

FIG. 2. (Color online) Nonlinear superposition of two ABs with two different modulation frequencies κ_j. (a) The frequency ratio is 2 : 1 with $\kappa_1 = 0.8$ and $\kappa_2 = 1.6$. (b) The frequency ratio is 3 : 2 with $\kappa_1 = 0.8$ and $\kappa_2 = 1.2$.

Notably, this technique for finding the rational limit works for any ratio of κ_j that is not one-to-one. As acknowledged in our previous work [26], a second-order rogue wave is generally built from three first-order Peregrine solitons. Therefore, enforcing a default 2 : 1 ratio with $\kappa_2 = 2\kappa_1$ allows us to obtain a solution where two component ABs form first-order triplets that merge into second-order peaks, provided that they share the same origin. This case is shown in Fig. 2(a). In contrast, a 3 : 2 ratio with $\kappa_2 = 1.5\kappa_1$, shown in Fig. 2(b), forms a series of triplets, which are merged together, alternating with distinct doublets. Similar structures repeating along the x axis appear in the KM soliton regime, although we caution that the integer ratios in this situation must be applied to $\delta_1 : \delta_2$ (or $\Omega_1 : \Omega_2$ in the real-parameter form), not $\kappa_1 : \kappa_2$. As Eq. (4) shows, this is because a KM soliton is periodic in x with a frequency of

$\Omega = -i\delta$ rather than κ. Nevertheless, in either case, the $\kappa \to 0$ limit isolates the single centrally located second-order rogue wave.

To see this merging of the triplet in greater detail, we present another particular case generated from the general two-breather solution in Eq. (7). This is the nonlinear superposition of an AB or a KM soliton with a Peregrine soliton and can be generated if we take the infinite period limit of one component independently of the other. Specifically, if $\kappa_1 \neq 0$ and $\kappa_2 \to 0$, then Eq. (7) reduces to a semirational expression (i.e., a mixture of polynomials with both trigonometric and hyperbolic functions in x and t):

$$
\begin{aligned}
G_2 &= \frac{\kappa_1}{8}\big(\kappa_1\big(\kappa_1^2\big(4x_{s2}^2 + 4t_{s2}^2 + 1\big) - 8\big)\cosh(\delta_1 x_{s1}) \\
&\quad + 8\delta_1 \cos(\kappa_1 t_{s1})\big), \\
H_2 &= \frac{\kappa_1}{4}\big(8x_{s2}\big(\delta_1 \cos(\kappa_1 t_{s1}) - \kappa_1 \cosh(\delta_1 x_{s1})\big) \\
&\quad + \delta_1\kappa_1\big(4x_{s2}^2 + 4t_{s2}^2 + 1\big)\sinh(\delta_1 x_{s1})\big), \qquad (8) \\
D_2 &= -\frac{1}{4\kappa_1}\big(\delta_1\big(\kappa_1^2\big(4x_{s2}^2 + 4t_{s2}^2 + 1\big) - 16\big)\cos(\kappa_1 t_{s1}) \\
&\quad + \kappa_1\big\{\big(\kappa_1^2\big(4x_{s2}^2 + 4t_{s2}^2 - 3\big) + 16\big)\cosh(\delta_1 x_{s1}) \\
&\quad - 16\delta_1[x_{s2}\sinh(\delta_1 x_{s1}) + t_{s2}\sin(\kappa_1 t_{s1})]\big\}\big).
\end{aligned}
$$

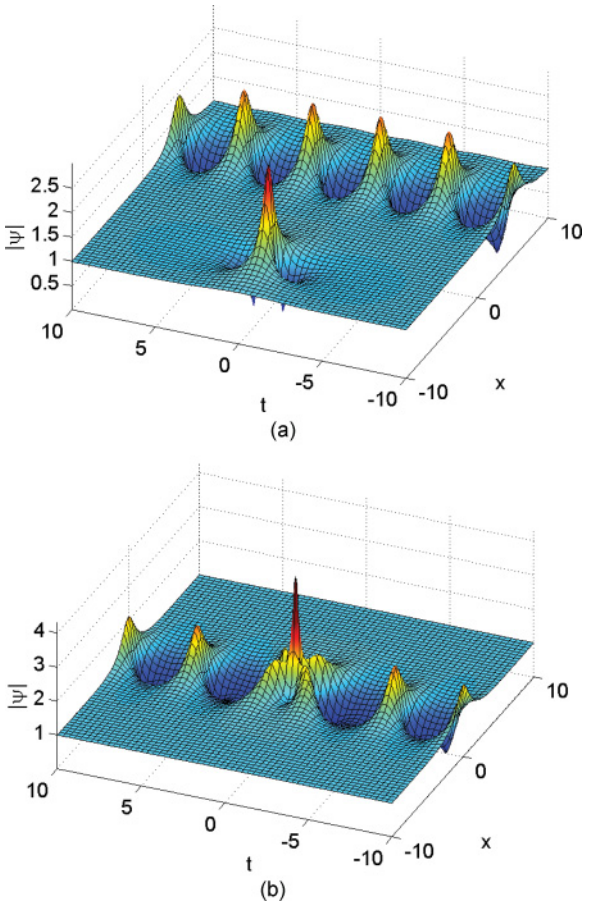

FIG. 3. (Color online) Nonlinear superposition of an AB ($l_1 = 0.65i$) with a Peregrine soliton ($l_2 = i$). (a) Shifts are $x_1 = 5$ and $x_2 = -5$. (b) Shifts are zero.

When the two components in this formula are well separated, the resulting solution appears as a Peregrine soliton and an AB (or a KM soliton), shown in Fig. 3(a). However, when these two components are nonlinearly overlaid, they appear as a first-order AB with a central second-order rogue wave peak, shown in Fig. 3(b). Three first-order peaks have effectively merged into a second-order peak. If we further apply the $\kappa_1 \to 0$ limit, we obtain the equation for a second-order rogue wave given below [see Eq. (10)]. This hybrid solution in Eq. (8) is thus one way to bridge the gap between a general second-order solution and an isolated rogue wave.

III. EQUAL-EIGENVALUE DEGENERATE SECOND-ORDER BREATHER

The general two-breather solution in Eq. (7) becomes undefined when the two eigenvalues l_1 and l_2 coincide. Despite this mathematical fact, numerical results similar to those in Fig. 2 show that, when the ratio of AB frequencies approaches 1 : 1, the solution appears as two almost parallel lines of periodically located peaks curving in at the origin to produce a second-order rogue wave in the center. In accordance with this observation, we set $x_1 = x_2 = t_1 = t_2 = 0$ and analytically apply the $\kappa_2 \to \kappa_1$ limit to Eq. (7). This can be done using a special form of l'Hôpital's rule. Specifically, we set $\kappa_1 = \kappa$ and $\kappa_2 = \kappa + \epsilon$, then Taylor expand both the numerator and denominator of $(G_2 + iH_2)/D_2$ in terms of ϵ. As all higher-order terms become zero at the $\epsilon \to 0$ limit, only the coefficients of the lowest-order terms in ϵ form the new numerator and denominator in the limiting solution.

This process results in the degenerate equal eigenvalue solution still given by Eq. (5), but now with real G_2, H_2, and D_2 given (again by mixtures of polynomials with trigonometric and hyperbolic functions in x and t) by

$$
\begin{aligned}
G_2 &= -\frac{2\kappa}{\delta}(\cosh(\delta x)((\delta^2 + \kappa^2)\cos(\kappa t) + \delta^2\kappa t\sin(\kappa t) \\
&\quad - 2\delta\kappa\cosh(\delta x)) + \cos(\kappa t)\sinh(\delta x)(2\delta^2 - \kappa^2)\delta x), \\
H_2 &= -\frac{1}{2\delta\kappa}(8\delta x(2\delta^2 - \kappa^2)[\delta\cos(\kappa t)\cosh(\delta x) - \kappa] \\
&\quad + 8\delta^3\sinh(\delta x)[\cos(\kappa t) + \kappa t\sin(\kappa t)] \\
&\quad + (\kappa^4 - 4\delta^2)\kappa\sinh(2\delta x)), \\
D_2 &= -\frac{1}{4\delta^2\kappa^2}(\kappa^4(\delta^2 + \kappa^2) + 8\delta^2\kappa^2(\delta^2 t^2 + \kappa^2 x^2) \\
&\quad + 32\delta^4 x^2(\delta^2 - \kappa^2) + 4[\kappa^4\cosh(2\delta x) - \delta^4\cos(2\kappa t)] \\
&\quad - 16\delta^2\kappa x(2\delta^2 - \kappa^2)\cos(\kappa t)\sinh(\delta x) \\
&\quad - 4\delta\kappa^2[4\delta^2 t\sin(\kappa t) + \kappa^3\cos(\kappa t)]\cosh(\delta x)), \qquad (9)
\end{aligned}
$$

where the lack of subscripts on κ and δ variables indicates that the two constituent components have equal parameters.

When using a real κ value, Eq. (9) represents two coincident ABs with equal eigenvalues, illustrated with the contour plot in Fig. 4(a). If κ is, instead, purely imaginary, then δ becomes imaginary and, as with Eq. (4), the trigonometric and hyperbolic functions swap via the relations in Eq. (3). In this case, localization in the x axis and periodicity in the t axis is replaced with localization in the t axis and periodicity in the x axis. The solution represents two coincident KM solitons with equal eigenvalues. It is illustrated in Fig. 4(b). In either situation, the

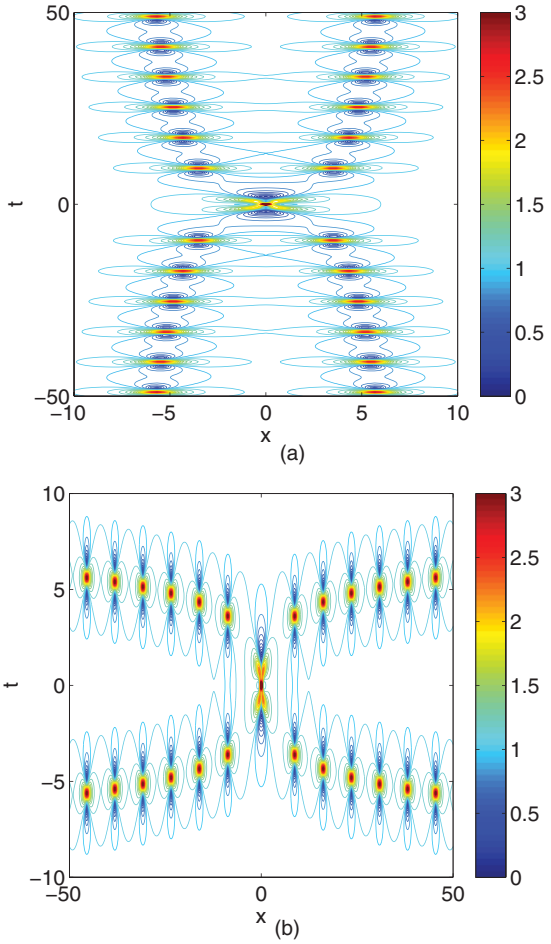

FIG. 4. (Color online) Contour plots of the two-breather solution $|\psi|$ in the equal eigenvalue limit. One axis in each plot is exaggerated in order to emphasise the curvature of the wave trains. The upper color bar limit does not signify the maximum amplitude. (a) Two ABs with equal $\kappa = 0.8$. (b) Two KM solitons with equal $\kappa = 0.8i$.

wave profile consists of two lines of peaks hinged upon one second-order rogue wave. This degenerate solution resembles the ordinary two-soliton degenerate solution presented in Fig. 3.15 of Ref. [37]. However, the difference is that the solution in Eq. (9) contains periodic structures that appear due to the presence of the background plane wave.

An interesting feature of the two solutions presented in Fig. 4 is that the location of the peaks almost coincide when one is rotated by 90° around the origin and overlaid on the other, even though the orientation of the substructures are kept unchanged (i.e., the pairs of troughs for each peak always line up along the t axis). This happens only when the coefficients of the NLSE are chosen to be those that we show in Eq. (1). In fact, most of the variation between peak alignment is due to the frequency of the periodic structures in an AB and a KM soliton being κ and $\Omega = -i\delta$, respectively. Thus the NLSE in this form has a remarkable symmetry, as has already been noted in our previous work [27].

Having the degenerate form of the two-breather solution in Eq. (9), we can use it to find the already familiar limit $\kappa \to 0$. This stretches the period of the wave train out to infinity, leaving at the center a single second-order rogue wave. The

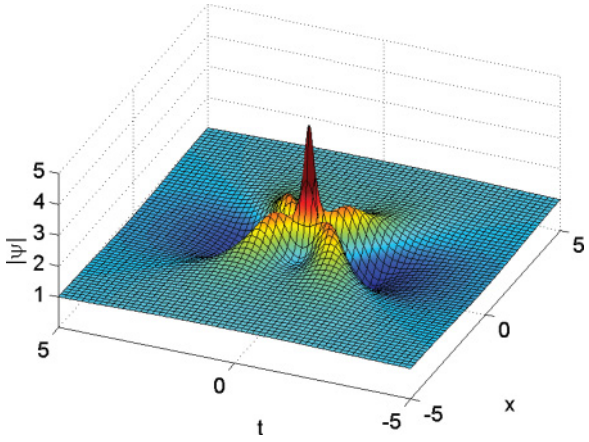

FIG. 5. (Color online) Second-order rogue wave given by Eq. (10).

resulting analytic expression is

$$
\begin{aligned}
G_2 &= \frac{1}{96}(80x^4 + 96x^2t^2 + 16t^4 + 72x^2 + 24t^2 - 3),\\
H_2 &= \frac{1}{48}x(16x^4 + 32x^2t^2 + 16t^4 + 8x^2 - 24t^2 - 15),\\
D_2 &= -\frac{1}{1152}(64x^6 + 192x^4t^2 + 192x^2t^4 + 64t^6 + 432x^4\\
&\quad -288x^2t^2 + 48t^4 + 396x^2 + 108t^2 + 9),
\end{aligned}
\tag{10}
$$

which gives the wave function shown in Fig. 5. Thus we have fully established the hierarchy of unshifted second-order breather solutions, ranging from the general case to the rogue wave via degenerate breathers.

IV. DIFFERENTIAL SHIFTS

Now the question is how to incorporate the shifted coordinates $x_{sj} = x - x_j$ and $t_{sj} = t - t_j$ into the equal eigenvalue limit. This is another highly nontrivial point in obtaining the limiting solutions and, as shown previously [27], the shifts need special consideration when eigenvalue limits are applied. Returning to the ϵ Taylor expansion process that turns Eq. (7) into Eq. (9), we realize that shifts cannot be arbitrary values independent of any other parameter. When $x_j \neq 0$ and $t_j \neq 0$ are treated as arbitrary, the lowest-order terms of G_2 and H_2, after Taylor expansion, are of order ϵ^1. However, the lowest-order term in D_2 is $4\delta^2\{\cos[\kappa(t_2 - t_1)] - \cosh[\delta(x_2 - x_1)]\}\epsilon^0$. This means that $(G_2 + iH_2)/D_2 = 0$ in the limit unless $t_1 = t_2$ and $x_1 = x_2$. This difficulty was also present when considering rogue wave clusters [27] and the only solution to this problem was to have shifts dependent on the limiting parameter. Specifically, we have to define $x_j = X_j\epsilon$ and $t_j = T_j\epsilon$. This definition changes the result of the ϵ expansion process, such that G_2, H_2, and D_2 have lowest-order terms of equal order in ϵ, thus avoiding a zero or infinite expression for $\epsilon \to 0$.

We caution that, as ϵ is defined to be proportional to κ in the Taylor expansion process, ABs and KM solitons have a real and imaginary value for ϵ, respectively. As x_j and t_j are always real-valued, pertaining to a shift of component origin in real space and time, then the nature of X_j and T_j consequently depends on ϵ. Specifically, these parameters are restricted to

being real for ABs and imaginary for KM solitons, otherwise singular solutions result.

When these definitions are taken into account, the degenerate equal eigenvalue limit becomes

$$
\begin{aligned}
G_2 = &-\frac{\kappa}{2\delta}[((8\delta^2+\kappa^4)\cos(\kappa t)+4\delta^2\kappa(t+\kappa T_d)\sin(\kappa t)\\
&-8\delta\kappa\cosh(\delta x))\cosh(\delta x)\\
&+4\delta[\delta^2(2x+\kappa X_d)-\kappa^2 x]\cos(\kappa t)\sinh(\delta x)],\\
H_2 = &-\frac{1}{2\delta\kappa}(8\delta[\kappa^2 x-\delta^2(2x+\kappa X_d)]\\
&\times[\kappa-\delta\cos(\kappa t)\cosh(\delta x)]+\kappa(\kappa^4-4\delta^2)\sinh(2\delta x)\\
&+8\delta^3[\cos(\kappa t)+\kappa(t+\kappa T_d)\sin(\kappa t)]\sinh(\delta x)),\\
D_2 = &-\frac{1}{4\delta^2\kappa^2}(\kappa^6+2\delta^2\kappa^2(\kappa^2(1+4x^2)-2)\\
&+8\delta^6(2x+\kappa X_d)^2+4\delta^4(1+2\kappa^2[(t+\kappa T_d)^2\\
&-2x(2x+\kappa X_d)]-\cos(2\kappa t))\\
&+\kappa[(4\delta^2+\kappa^4)\kappa\cosh(2\delta x)\\
&-16\delta^3\kappa(t+\kappa T_d)\cosh(\delta x)\sin(\kappa t)\\
&+4\delta\cos(\kappa t)(4\delta[\kappa^2 x-\delta^2(2x+\kappa X_d)]\sinh(\delta x)\\
&-\kappa^4\cosh(\delta x))]),
\end{aligned}
\tag{11}
$$

where we define the differential shifts as $X_d = X_1 - X_2$ and $T_d = T_1 - T_2$. Again we stress that the differential shifts have imaginary values in the KM soliton regime, although naturally $|X_d|$ and $|T_d|$ always represent the magnitude of the differential shifts. To avoid confusion, we will henceforth examine degenerate ABs, although the conclusions drawn have close analogues in the KM soliton case.

The first feature revealed by Eq. (11) is that a differential shift T_d along the t axis of the degenerate two-breather solution, shown in Fig. 4, does not change the overall structure of the wave profile. Two first-order ABs remain symmetrically arrayed and held in close proximity with a single intersection. However, the nature of this point of intersection depends on the value of the differential shift. It may change if the two breather components with equal eigenvalues are shifted relative to each other, at which point the perfect peak alignment in the middle of the intersection disappears. This case is shown in Fig. 6(a). The intersection more closely resembles the rogue wave triplet [26] than a second-order rogue wave with a single peak. However, periodicity of the solution suggests that the latter arrangement can be restored at specific values of T_d and its multiples. Indeed, Fig. 6(b) shows that the high peak appears again at a nonzero value of differential shift T_d.

The differential shift X_d has a different effect on the solution with equal eigenvalues. As shown in Fig. 7(a), the intersection point starts to disappear when X_d takes nonzero values. For a sufficiently large shift, the two first-order components are separated and the intersection disappears completely. This case is shown in Fig. 7(b). However, the interaction between the two breathers is still surprisingly strong. As a result, the two components are organized in an interleaving zigzag structure. Such an asymmetric arrangement appears to be a direct consequence of the $\epsilon \to 0$ limit. Indeed, taking the limit with κ_2 set as $\kappa - \epsilon$ instead of $\kappa + \epsilon$ is likely to flip the zigzag structure. However, we reiterate that the absolute shifts $x_j = X_j\epsilon$ and $t_j = T_j\epsilon$ are still technically zero in this limit, irrespective of the X_j and T_j values, and this may be vital in explaining why the two breathers do not repel each other to the infinity horizon of the (x,t) plane.

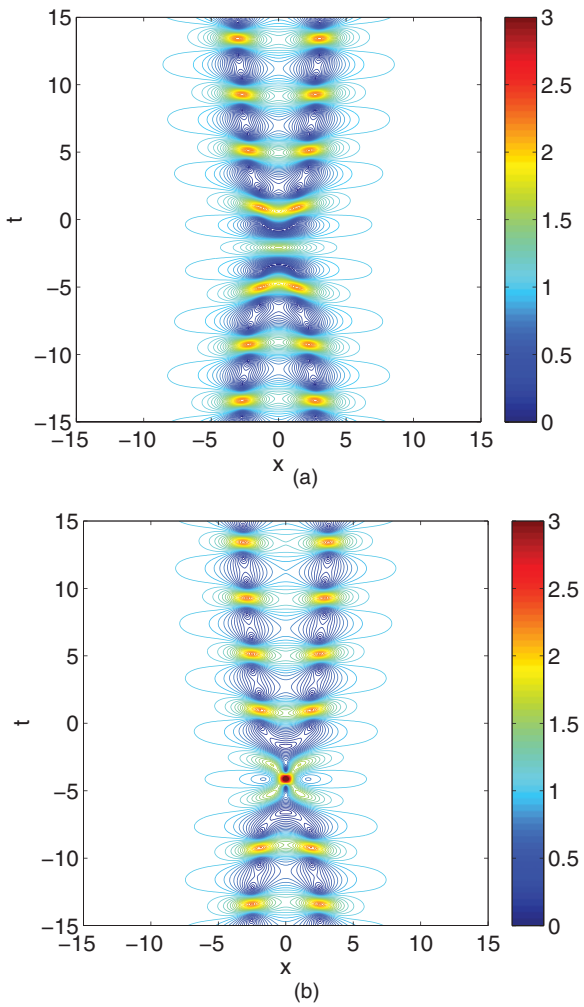

FIG. 6. (Color online) Contour plots of the two-breather solution $|\psi|$ in the degenerate limit, with $l = 0.65i$ and a nonzero differential shift T_d between the two components. The upper color bar limit does not signify the maximum amplitude. (a) $T_d = 0.9\kappa$. (b) $T_d = 1.8\kappa$.

Linking this result to already known solutions, the $l \to i$ ($\kappa \to 0$) limit of Eq. (11), with any value of the differential shift applied, is expected to produce a rogue wave triplet [26]. However, as κ approaches zero and the period of the breathers becomes infinite, keeping the values of X_d and T_d constant is not sufficient to prevent the components from repelling each other to infinity. Instead, we define $X_d = x_d\kappa$ and $T_d = t_d\kappa$, which alternatively allows the difference between absolute shifts to be written in full as $x_1 - x_2 = x_d\kappa\epsilon$ and $t_1 - t_2 = t_d\kappa\epsilon$. Fixed values of x_d and t_d keep the circumradius of the rogue wave triplet constant, even when it is the only structure left at the origin of the (x,t) plane in the $\kappa \to 0$ limit. An example of this process with two KM solitons is shown in Fig. 8. Furthermore, unlike X_d and T_d, the values of x_d and t_d are always real, even in the KM soliton regime, as $\kappa\epsilon$ is always real. In any case, the second-order breather solution with equal eigenvalues can be considered as an intermediate

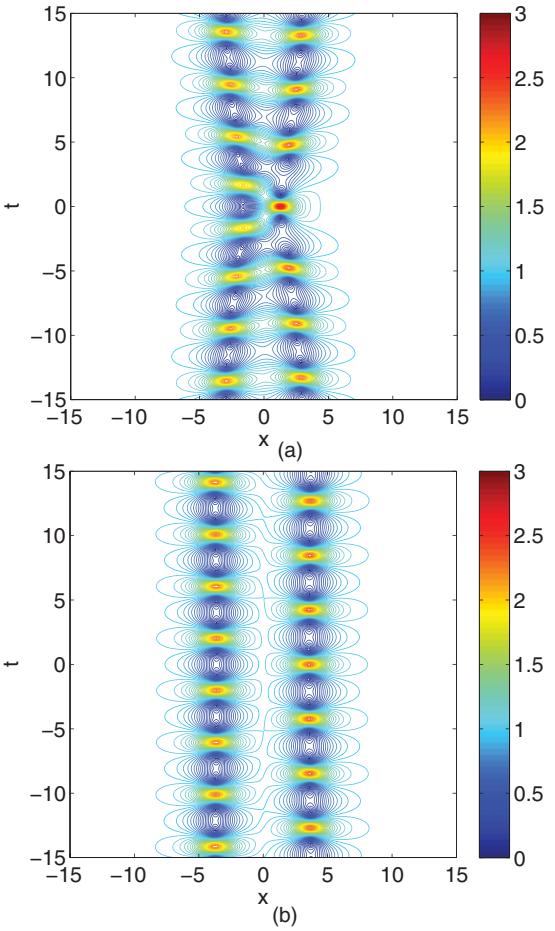

FIG. 7. (Color online) Contour plots of the two-breather solution $|\psi|$ in the degenerate limit, with $l = 0.65i$ and a nonzero differential shift X_d between the components. The upper color bar limit does not signify the maximum amplitude. (a) $X_d = 1.8\kappa$. (b) $X_d = 18\kappa$.

link between pure rogue waves and the general second-order breather solutions given by Eq. (7).

Direct analytic application of the $\kappa \to 0$ limit to Eq. (11) generates the following solution

$$
\begin{aligned}
G_2 &= \frac{1}{96}(80x^4 + 96x^2t^2 + 16t^4 + 72x^2 - 192xx_d \\
&\quad + 24t^2 - 192tt_d - 3), \\
H_2 &= \frac{1}{48}(16x^5 + 32x^3t^2 + 16xt^4 + 8x^3 - 96x^2x_d \\
&\quad - 24xt^2 + 96x_dt^2 - 192xtt_d - 15x + 24x_d), \\
D_2 &= -\frac{1}{1152}(64x^6 + 192x^4t^2 + 192x^2t^4 + 64t^6 \\
&\quad + 432x^4 - 768x^3x_d - 288x^2t^2 + 2304xx_dt^2 \\
&\quad - 2304x^2tt_d + 48t^4 + 768t^3t_d + 396x^2 - 1728xx_d \\
&\quad + 2304x_d^2 + 108t^2 - 576tt_d + 2304t_d^2 + 9). \qquad (12)
\end{aligned}
$$

This is the same solution for the shifted second-order rogue wave given previously [22–24,27], although x_d and t_d here have a different scaling factor of 2/3. This minor difference is due to the rogue wave limit in this work being taken with a different frequency ratio between components. Indeed, had $\kappa_1 : \kappa_2$ been, for example, 1 : 3 rather than 1 : 2 in the previous derivation [27], x_d and t_d would have been scaled differently yet again. Nonetheless, as ϵ is of order κ, the process described in this work still supports the claim that a second-order rogue wave requires shifts proportional to κ^2 in order to be transformed into a triplet of finite circumradius in the $\kappa \to 0$ limit [27].

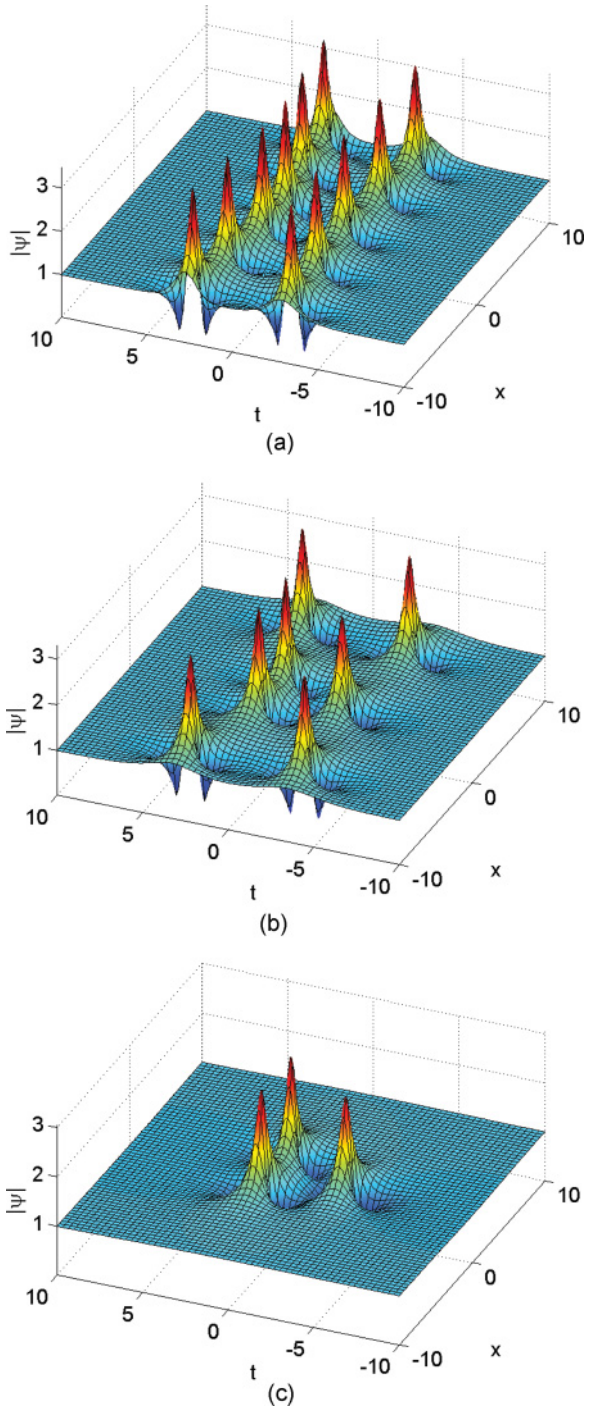

FIG. 8. (Color online) Two KM solitons with equal eigenvalues, given by Eq. (11). The differential shift is $T_d = 3\kappa$ ($t_d = 3$) in all three cases. The two equal eigenvalues are (a) $l = 1.2i$. (b) $l = 1.1i$. (c) $l \approx i$. The period of the two breathers approaches infinity when the eigenvalues tend to i.

V. CONCLUSION

In summary, our main results are as follows.

i) We have found a general analytic expression for the two-breather solution of the NLSE with two independent imaginary eigenvalues. This solution describes nonlinearly superimposed ABs or KM solitons as well as their combinations.

ii) We have found the nontrivial degenerate solution in the limit of equal eigenvalues. Where simple substitution leads to an undefined expression, special application of l'Hôpital's rule allows the solution to be presented in explicit form. We illustrated this solution with two cases where the component breathers are either ABs or KM solitons. The analysis shows that in each case, these degenerate solutions consist of two near-parallel lines almost periodic in structure, with only one point of intersection.

iii) We introduced two free parameters, differential shifts between components, that modify the structure of the degenerate solution. We studied the wave profile at the point of intersection and how it is influenced by these parameters. In particular, the profile varies between the single-peak second-order rogue wave and the three-peak rogue wave triplet, depending solely on the value of the differential shifts.

iv) We have found that the rogue wave limit of infinite period, when the two equal eigenvalues are equal to i, generates the familiar second-order rogue wave with two free parameters; differential shifts along the t and x axes.

Ultimately, we have established how these wave functions are all related in a hierarchy of second-order breather solutions. This concept has previously been obtuse, at best. The degenerate solutions are in effect a missing link between arbitrary superpositions and rogue waves. This understanding is particularly significant as analytic expressions for higher orders become vastly more complex, even for simple rogue wave limits [23]. Second order is potentially the final regime where the hierarchy of all structures can be efficiently described. Even so, multibreather solutions that appear in a chaotic wave field can still be studied in a similar way as presented. The analysis here gives a good qualitative description of the higher-order structures expected to be generated. Numerics demonstrate, as shown in Fig. 9 with a fifth-order rogue wave produced in the intersection of five KM solitons, that this is potentially a way to produce very high amplitude waves from much smaller structures, without resorting to ideal rogue waves with infinite period.

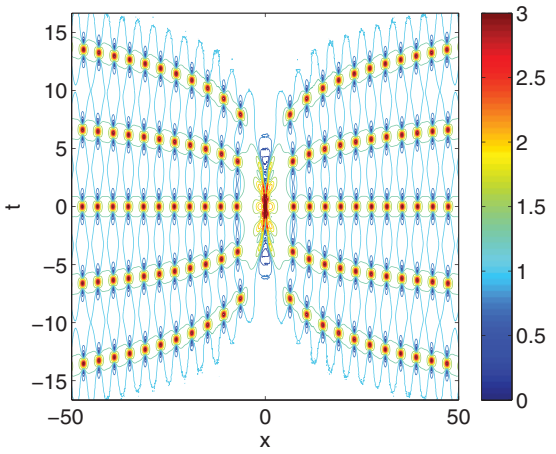

FIG. 9. (Color online) Numerical contour plot of the five-breather solution $|\psi|$ near the equal eigenvalue limit, with $l \approx 1.2i$ for all KM solitons. One axis is exaggerated to emphasize the curvature of the wave trains. The upper color bar limit does not signify the maximum amplitude.

One of the important applications of our results is related to the description of the higher-order modulation instability of constant amplitude waves [38]. Varying two independent frequencies within the instability band may create significantly more complicated controllable periodic structures as a result of modulation instability [39]. We have already mentioned higher amplitude peaks within each period of modulation, but the amplitude profile within each period may also vary and can be tailored by adjusting the modulation depth and delay between the two frequency components. These experiments can be conducted either with water waves or in optics. Thus our explicit solutions may significantly enrich the family of pulse sequences and wave shapes that can be generated in fiber and water tanks, respectively. The seminal experiments have already been completed [9,12] and we expect further progress in this exciting area of research.

ACKNOWLEDGMENTS

The authors acknowledge the support of the Australian Research Council (Discovery Project No. DP110102068). N.A. and A.A. acknowledge support from the Volkswagen Stiftung.

[1] D. Peregrine, J. Austral. Math. Soc. Ser. B **25**, 16 (1983).
[2] K. B. Dysthe and K. Trulsen, Phys. Scr., T **82**, 48 (1999).
[3] A. R. Osborne, *Nonlinear Ocean Waves and the Inverse Scattering Transform* (Elsevier, Amsterdam, 2010).
[4] E. Pelinovsky and C. Kharif, *Extreme Ocean Waves* (Springer, Berlin, 2008).
[5] V. V. Voronovich, V. I. Shrira, and G. Thomas, J. Fluid Mech. **604**, 263 (2008).
[6] V. Shrira and V. Geogjaev, J. Eng. Math. **67**, 11 (2010).
[7] I. Ten and H. Tomita, Reports of RIAM Symposium, Kasuga, Fukuoka, Japan, 2006, Report No. 17SP1-2.
[8] C. Garrett and J. Gemmrich, Phys. Today **62**(6), 62 (2009).
[9] A. Chabchoub, N. P. Hoffmann, and N. Akhmediev, Phys. Rev. Lett. **106**, 204502 (2011).
[10] V. B. Efimov, A. N. Ganshin, G. Kolmakov, P. McClintock, and L. Mezhov-Deglin, Eur. Phys. J. Spec. Top. **185**, 181 (2010).
[11] M. Shats, H. Punzmann, and H. Xia, Phys. Rev. Lett. **104**, 104503 (2010).

[12] B. Kibler, J. Fatome, C. Finot, G. Millot, F. Dias, G. Genty, N. Akhmediev, and J. M. Dudley, Nature Phys. **6**, 790 (2010).
[13] N. Akhmediev, V. I. Korneev, and N. V. Mitskewich, Zh. Experimentalnoii i Teoreticheskoii Fiziki (USSR) **94**, 159 (1988) [Sov. Phys. JETP, **67**, 89 (1988)].
[14] N. Akhmediev, J. M. Soto-Crespo, and A. Ankiewicz, Phys. Lett. A **373**, 2137 (2009).
[15] N. Akhmediev, J. M. Soto-Crespo, and A. Ankiewicz, Phys. Rev. A **80**, 043818 (2009).
[16] N. Akhmediev and A. Ankiewicz, Opt. Commun. **100**, 186 (1993).
[17] L. Gagnon and N. Stevenart, Opt. Lett. **19**, 619 (1994).
[18] V. B. Matveev and M. Salle, *Darboux Transformations and Solitons* (Springer-Verlag, Berlin, 1991).
[19] N. Akhmediev, A. Ankiewicz, and M. Taki, Phys. Lett. A **373**, 675 (2009).
[20] N. Akhmediev, A. Ankiewicz, and J. M. Soto-Crespo, Phys. Rev. E **80**, 026601 (2009).
[21] P. Dubard, P. Gaillard, C. Klein, and V. Matveev, Eur. Phys. J. Spec. Top. **185**, 247 (2010).
[22] P. Gaillard, Institut National des Sciences Mathématiques et de Leurs Interactions, Report No. halshs-00536287, 2010 (unpublished).
[23] P. Gaillard, Institut de Mathématiques de Bourgogne, Report No. hal-00573955, 2011 (unpublished).
[24] P. Gaillard, J. Phys. A: Math. Theor. **44**, 435204 (2011).
[25] P. Dubard and V. B. Matveev, Natural Hazards and Earth System Sciences **11**, 667 (2011).
[26] A. Ankiewicz, D. J. Kedziora, and N. Akhmediev, Phys. Lett. A **375**, 2782 (2011).
[27] D. J. Kedziora, A. Ankiewicz, and N. Akhmediev, Phys. Rev. E **84**, 056611 (2011).
[28] N. Akhmediev and V. I. Korneev, Teoreticheskaya i Matematicheskaya Fizika (USSR) **69**, 189 (1986) [Theor. Math. Phys. **69** 1089 (1986)].
[29] N. Akhmediev, V. M. Eleonskii, and N. E. Kulagin, Theoreticheskaya i Mathematicheskaya Fizika (USSR) **72**, 183 (1987) [Theoretical and mathematical physics **72**, 809 (1987)].
[30] M. Tajiri and Y. Watanabe, Phys. Rev. E **57**, 3510 (1998).
[31] Q.-Han Park and H. J. Shin, Phys. Rev. Lett. **82**, 4432 (1999).
[32] S. L. Lu Li, Zhonghao Li and G. Zhou, Opt. Commun. **234**, 169 (2004).
[33] V. Zakharov and A. Gelash, arXiv:1109.0620v2 (2011).
[34] N. Akhmediev, V. M. Eleonskii, and N. E. Kulagin, Zh. Eksperimentalnoii i Teoreticheskoii Fiziki **89**, 1542 (1985) [Sov. Phys. JETP **62**, 894 (1985)].
[35] E. A. Kuznetsov, Dokl. Akad. Nauk SSSR **236**, 575 (1977) [Sov. Phys. Dokl. **22**, 507 (1977)].
[36] Y.-C. Ma, Stud. Appl. Math. **60**, 43 (1979).
[37] N. Akhmediev and A. Ankiewicz, *Solitons: Nonlinear Pulses and Beams*, Vol. 5 of *Optical and Quantum Electronics* (Chapman & Hall, London, 1997), Chap. 3–4.
[38] S. Wabnitz and N. Akhmediev, Opt. Commun. **283**, 1152 (2010).
[39] M. Erkintalo, K. Hammani, B. Kibler, C. Finot, N. Akhmediev, J. M. Dudley, and G. Genty, Phys. Rev. Lett. **107**, 253901 (2011).